A protocol to realize triatomic ultralong range Rydberg molecules in an ultracold KRb gas

Rosario González-Férez[1] ⬤**, Seth T Rittenhouse**[2]**,**
Peter Schmelcher[3,4] ⬤ **and H R Sadeghpour**[5] ⬤

[1] Instituto Carlos I de Física Teórica y Computacional and Departamento de Física Atómica, Molecular y Nuclear, Universidad de Granada, E-18071 Granada, Spain
[2] Department of Physics, The United States Naval Academy, Annapolis, MD 21402, United States of America
[3] Zentrum für Optische Quantentechnologien, Universität Hamburg, Luruper Chaussee 149, D-22761 Hamburg, Germany
[4] The Hamburg Centre for Ultrafast Imaging, Universität Hamburg, Luruper Chaussee 149, D-22761 Hamburg, Germany
[5] ITAMP, Harvard-Smithsonian Center for Astrophysics 60 Garden St., Cambridge, MA 02138, United States of America

E-mail: rogonzal@ugr.es

CrossMark

Abstract

We propose an experimentally realizable scheme to produce triatomic ultralong-range Rydberg molecules (TURM), formed in ultracold KRb traps. A near resonant coupling of the non-zero quantum defect Rydberg levels with the KRb molecule in $N = 0$ and $N = 2$ rotational levels, is engineered which exploits the unique Rydberg electron–molecule anisotropic dipole interaction. This near resonant coupling enhances the TURM binding and produces favorable Franck–Condon factors. Schemes for both potassium and rubidium excitations are demonstrated.

Keywords: Rydberg molecules, Rydberg atoms, ultralong-range

(Some figures may appear in colour only in the online journal)

1. Introduction

Rydberg atoms are superb probes of their environments. Spectral shift and broadening of Rydberg lines in thermal gases have been used for temperature and density diagnostics of atomic and molecular laboratory and astrophysical gases [1–3], and were instrumental in the early development of low-energy atomic collision physics [4]. The advent of ultracold trapping and cooling techniques now permit routine probes of environmental bath in the quantum limit [5–8].

Ultracold molecules offer another intriguing toolkit for manipulation and control of interatomic and atom–molecule interactions [9]. Ultracold molecules possessing permanent electric dipole moments are particularly in vogue for a host of applications in ultracold chemistry, quantum information processing and many-body quantum physics.

The interaction of a Rydberg atom with a non-degenerate ground state atom is best described as the quasi-free electron scattering at low energy from pertuber atoms. When the electron de Broglie wavelength is large compared with other interaction length scales, the Fermi pseudopotential method was invoked for binding of a Rydberg atom with a bath atom, forming Rydberg molecules bound at ultra-long separations [10–13]. When the environmental gas is comprised of molecules possessing permanent electric field dipole moments, the low-energy Rydberg electron scattering is best described as the charge-dipole interaction [14]. This interaction has a critical value- the Fermi–Teller critical dipole moment $d_c \approx 1.63$ Debye; molecules with supercritical dipole moments may bind electrons and create anions and those with subcritical dipole moments scatter electrons [15–17].

The original proposal for creation of ultralong range triatomic Rydberg molecules (TURM) comprised of a Rydberg atom and a polar molecule [18], imagined a two-level polar molecule, say the opposite-parity electronic doublet in OH interacting with a Rydberg electron. Subsequent calculations expanded upon the original proposal to successively incorporate rotational molecules and their linear response with electric fields [19–21]. Interesting aspects of these molecules are their prodigious permanent electric dipole moments, sensitivity to small external electric field, and the existence of multiple, state-dependent orientations of the molecules [21]. The full rotational level structure in the ground state polar molecule was incorporated in [20, 22].

Ultralong range triatomic molecules discussed here and above have utility beyond Rydberg chemistry, such as coherently oriented molecules, and for quantum information processing and simulation of magnetic impurity interactions. Specific examples include Rydberg mediated conditional molecular gates and their non-destructive readouts [23, 24] and simulation of indirect spin–spin interactions [25] in bilayers of Rydberg atoms and rotational polar molecules. In many such examples, the existence of large dipole moments is a blessing [26].

Here, we detail with accurate calculations, an unexplored near resonant scheme between rotational and Rydberg levels, which we show is most optimal for experimental realization. In all previous calculations, the most interesting triatomic molecular states were those associated with the nearly degenerate manifold of high angular momentum Rydberg states. In each case, the molecules were predicted to have little to no *s*- or *d*-wave Rydberg character [21, 20] making them inaccessible to conventional two-photon Rydberg excitation schemes. We leverage the rotational structure in the ground vibrational state of KRb molecules to find advantageous *s* or *d* Rydberg orbital admixtures for the experimental realization of ultralong range triatomic Rydberg molecules.

We consider a mixture of ultracold potassium ^{39}K and rubidium atoms ^{87}Rb, where ultracold extremely weakly bound Feshbach ^{39}K^{87}Rb molecules are formed by magnetoassociation [27]. These extremely weakly bound molecules are transferred to the electronic and vibrational ground-state by a coherent two-photon Raman scheme, which creates KRb molecules in either $N = 0$ or $N = 2$ rotational state [27]. The rotational constant of KRb is $B = 1.114$ GHz [28], and its electric dipole moment is subcritical, $d = 0.566$ Debye.

In such a atom–molecule mixture, either potassium or rubidium atoms could be excited into *nd* or *ns* Rydberg states by standard two-photon absorption schemes. If the KRb molecule is found in the Rydberg orbit, the TURM molecules, K–KRb or Rb–KRb, were predicted to form [18, 19, 21]. In the previous attempts, [20, 22], we showed that the adiabatic electronic potential curves (APC) evolving from the *nd* or *ns* Rydberg thresholds are deep enough to accommodate several vibrational bound states, but the corresponding vibrational spacing to be smaller than 1 MHz, and therefore beyond spectroscopic resolution. In addition, the potential energy surfaces associated with these states are likely to be highly sensitive to the *s*-wave scattering length associated with the

electron-KRb polarization interaction, a quantity that is currently not known.

In contrast, the adiabatic potential energy curves evolving from the Rydberg degenerate manifolds, i.e. $l \gtrsim 3$, exhibit potential wells with few GHz depths [20], and, the corresponding vibrational bound states can be resolved spectroscopically. Furthermore, the electron–molecule interaction is dominated by the charge-dipole interaction. The Rydberg degenerate manifold could be accessed experimentally from the neighboring *ns* or *nd* Rydberg state, allowing for the creation of the TURM molecules.

2. The theoretical protocol

Our aim is to suggest an experimentally viable scheme for the production of the TURM in an adiabatic electronic potential evolving from a *ns* or *nd* Rydberg state, by coupling these electronic states to those evolving from a hydrogenic-like degenerate manifold. The goal is to enhance the depth of these APC, and, therefore, the energy spacing of the vibrational bound states, by coupling these quantum defect states to the closest degenerate manifold using the dipole interaction with the polar diatomic molecule.

To engineer such a coupling, the energy splitting of the *ns* or *nd* Rydberg state from the neighboring degenerate manifold, i.e. $|E(n's) - E(n, l > 3)|$ or $|E(n'd) - E(n, l > 3)|$, should be close to but larger than the energy of a given rotational excited state of the field-free KRb molecule. Thus, and taking as an example the excitation of potassium, the APC of the K$(n + 2, s)$–KRb$(N > 0)$ or K(n, d)–KRb$(N > 0)$ TURM should be immersed among the APCs of K$(n, l > 3)$–KRb$(N = 0)$, i.e. the APC evolving from the Rydberg degenerate manifold with principal quantum number n and KRb in its rotational ground-state $N = 0$. We note that due to interaction with the core electrons, Rydberg valence electron energies are shifted from the hydrogenic levels; the usual terminology is that the levels obtain a quantum defect $E_{nl} = -\frac{R_\infty}{(n - \mu_l)}$, where R_∞ is the Rydberg constant and μ_l is the *l*-dependent quantum defect. With each additional orbital angular momentum, μ_l becomes smaller such that for *l* larger than some value, here $l \geqslant 3$, $\mu_l \sim 0$; hence the degenerate manifold.

For potassium, figure 1(a) shows the energy shifts $|E(n + 2, s) - E(n, l > 3)|$ and $|E(n, d) - E(n, l > 3)|$ versus the quantum number *n*. In this figure, the rotational excited states of KRb are represented by the horizontal lines. The possible Rydberg manifold candidates to engineer the coupling are given by the principal quantum number *n* having an energy slight larger than one of the horizontal lines. For instance, the $51 \lesssim n \lesssim 56$ ($59 \lesssim n \lesssim 64$) degenerate manifolds of potassium are good candidates to create the TURM via the K$((n + 2)s)$ (K(nd)) quantum-defect Rydberg state and KRb $(N = 2)$, i.e. the Rydberg states to left of the crossings marked by a circle in figure 1 (a). The corresponding results for exciting the rubidium atom are shown in figure 1(b). For Rb, the $45 \lesssim n \lesssim 50$ ($64 \lesssim n \lesssim 69$) degenerate manifolds are good candidates to create the TURM via the dipole coupling of the
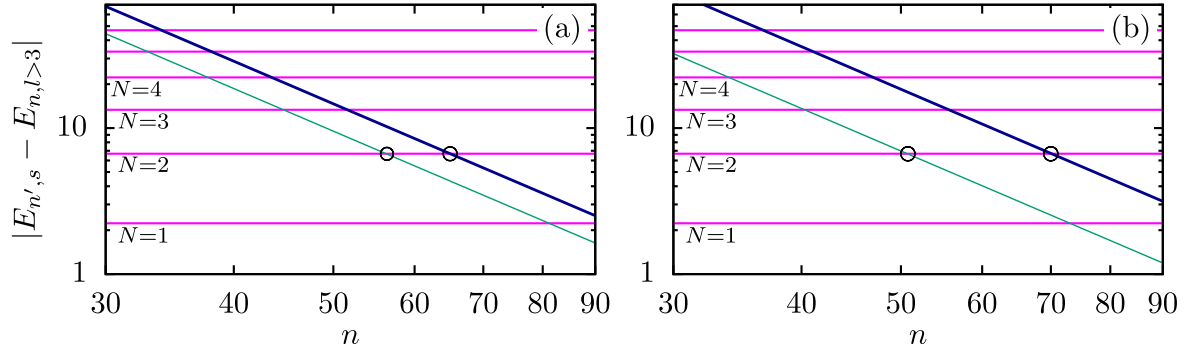
Figure 1. (a) For potassium, energy splittings in GHz of the Rydberg states K$((n + 2)s)$ (thin green line) and K(nd) (thick blue line) from the neighboring Rydberg manifold K$(n, l \geqslant 3)$ as a function of the principal quantum number n. (b) For rubidium energy splittings in GHz of the Rydberg states Rb$((n + 3)s)$ (thin green line) and Rb$((n + 1)d)$ (thick blue line) from the neighboring Rydberg manifold Rb$(n, l \geqslant 3)$ versus the principal quantum number n. The horizontal lines represent the energies of the rotationally excited states of KRb. The crossings between these Rydberg energies and the $N = 2$ rotational state of KRb are marked with a circle, the Rydberg states to the left of these crossings are potential candidates to form the TURM.

Rb$((n + 3)s)$ (Rb$((n + 1)d)$) Rydberg state and KRb$(N = 2)$, see figure 1(b).

The rest of this paper is organized as follows. In section 3 we present the theoretical method. The APC of two Rydberg molecules K–KRb and Rb–KRb are discussed and analyzed in section 4. Our conclusions are provided in section 5.

3. The TURM Hamiltonian

We consider a triatomic molecule (TURM) formed by a Rydberg atom and a ground state heteronuclear diatomic molecule. The diatomic molecule is described within the Born–Oppenheimer and rigid rotor approximations. The Rydberg atom is represented by an effective single-electron system. In this framework, the adiabatic Hamiltonian is

$$H_{ad} = H_A + H_{mol}, \tag{1}$$

where H_A represents the single electron Hamiltonian describing the Rydberg atom

$$H_A = -\frac{\hbar^2}{2m_e}\nabla_r^2 + V_l(r), \tag{2}$$

where $V_l(r)$ is the l-dependent model potential [29], with l being the angular momentum quantum number of the Rydberg electron with respect to its positively charged core.

The molecular Hamiltonian describing the rigid rotor molecule and the charge-dipole interaction reads

$$H_{mol} = B\mathbf{N}^2 - \mathbf{d} \cdot \mathbf{F}_{ryd}(\mathbf{R}, \mathbf{r}) \tag{3}$$

with B being the rotational constant, $\mathbf{N}$ the molecular angular momentum operator and $\mathbf{d}$ the permanent electric dipole moment of the diatomic molecule. $\mathbf{F}_{ryd}(\mathbf{R}, \mathbf{r})$ is the electric field due to the Rydberg electron and the ion at position $\mathbf{R}$

$$\mathbf{F}_{ryd}(\mathbf{R}, \mathbf{r}) = e\frac{\mathbf{R}}{R^3} + e\frac{\mathbf{r} - \mathbf{R}}{|\mathbf{r} - \mathbf{R}|^3}, \tag{4}$$

where e is the electron charge, $\mathbf{r}$ is the position of the Rydberg electron, and $\mathbf{R}$ is the position of the diatomic molecule with respect to the Rydberg core. The KRb molecule is in its

ground electronic state, i.e. X$^1\Sigma$, whose electronic spin is zero and therefore does not introduce spin-exchange mixing of the electronic states. The presence of both hyperfine and electron-quadrupole interactions will introduce only a weak mixing and small shifts in the APCs and are therefore neglected here. The rovibrational motion is treated in the rigid rotor approximation and the rotational constant is $B = 1.114$ GHz.

We consider the position of the Rydberg core fixed at the center of the coordinate system of the laboratory fixed frame, and the diatomic molecule is located at the Z-axis, i.e. $\mathbf{R} = R\hat{Z}$. By fixing the distance between the diatomic molecule and the Rydberg core R, we solve the Schrödinger equation associated with the Hamiltonian (1) and obtain the adiabatic electronic potential curves (APC) as a function of R. In the limit of very large separations, the interaction between the Rydberg atom and KRb tends to zero, and the APC approaches the energies of the two non-interacting species, i.e. $E_{n,l} + N(N + 1)B$, with $E_{n,l}$ being the energy of the corresponding Rydberg state, and $N(N + 1)B$ the rotational energy of the KRb molecule in its electronic and vibrational ground-state.

To solve the Schrödinger equation associated with the Hamiltonian (1), we perform a basis set expansion in terms of the coupled basis

$$\Psi(\mathbf{r}, \Omega; R) = \sum_{n,l,N,J} C_{n,l,m}^J(R)\Psi_{nl,N}^{JM_J}(\mathbf{r}, \Omega), \tag{5}$$

where the sum in J satisfies $|l - N| \leqslant J \leqslant l + N$, and

$$\Psi_{nl,N}^{JM_J}(\mathbf{r}, \Omega) = \sum_{m_l=-l}^{m_l=l}\sum_{M_N=-N}^{M_N=N}$$
$$\times \langle lm_l NM_N|JM_J\rangle Y_{NM_N}(\Omega)\psi_{nlm}(\mathbf{r}) \tag{6}$$

with $\langle lm_l NM_N|JM_J\rangle$ being the Clebsch–Gordan coefficient, $J = |l - N|,...,l + N$, and $M_J = -J, ..., J$. $\psi_{nlm}(\mathbf{r})$ is the Rydberg electron wave function with n, l and m being the principal, orbital and magnetic quantum numbers, respectively, and $Y_{NM_N}(\Omega)$ is the field-free rotational wave function of the diatomic molecule. The total angular momentum of the Rydberg molecule, excluding an overall rotation, is given by $\mathbf{J} = \mathbf{l} + \mathbf{N}$, where $\mathbf{l}$ is the orbital angular momentum of the Rydberg electron, and $\mathbf{N}$ is the molecular rotational angular momentum of the diatomic molecule. Here, we include

rotational excitations of KRb up to $N \leqslant 5$, and for the Rydberg wave functions, we include the degenerate manifold with $l > 3$, and the neighboring quantum defect states with $l = 0$, 1, 2, 3. In this work, we focus on the states with $M_J = 0$, i.e. $M_N + m_l = 0$, and the basis is formed by 2142 and 2632 coupled states for $n = 46$ and $n = 56$, respectively.

To gain physical insight into the features of these exotic molecules, we compute their electric dipole moment as

$$D_{ryd}(R) = \langle \Psi | r \cos \theta_e | \Psi \rangle$$
$$= \int \Psi^*(\mathbf{r}, \Omega; R) r \cos \theta_e \Psi(\mathbf{r}, \Omega; R) d\mathbf{r} d\Omega, \quad (7)$$

where θ_e is the polar angle of the Rydberg electron. This integral is non-zero if there are partial waves with different parity, i.e. $\Delta l = \pm 1$, contributing to the wave function (5). We also explore the orientation and alignment of the KRb molecule within the TURM given by

$$O_{ryd}(R) = \langle \Psi | \cos \theta | \Psi \rangle$$
$$= \int \Psi^*(\mathbf{r}, \Omega; R) \cos \theta \Psi(\mathbf{r}, \Omega; R) d\mathbf{r} d\Omega, \quad (8)$$

$$A_{ryd}(R) = \langle \Psi | \cos^2 \theta | \Psi \rangle$$
$$= \int \Psi^*(\mathbf{r}, \Omega; R) \cos^2 \theta \Psi(\mathbf{r}, \Omega; R) d\mathbf{r} d\Omega. \quad (9)$$

The weight of a certain rotational state of KRb in the TURM wave function (5) reads

$$\mathcal{C}_N(R) = \sum_{n,l,J} |C^J_{n,l,m}(R)|^2 \text{ satisfying } \sum_N \mathcal{C}_N(R) = 1, \quad (10)$$

and the weight of a certain partial wave of the Rydberg electron is

$$\mathcal{C}_{n,l}(R) = \sum_{N,J} |C^J_{n,l,m}(R)|^2 \text{ satisfying } \sum_{n,l} \mathcal{C}_{n,l}(R) = 1. \quad (11)$$

For the sums of these two previous expressions, it holds $|l - N| \leqslant J \leqslant l + N$.

The TURMs exist, if an APC can accommodate vibrational bound states. The corresponding vibrational spectrum is obtained by solving the Schrödinger equation associated to a given APC. We estimate the probability to create these TURMs by photoassociation via the Franck–Condon factor weighted with the $l = 0$, $N = 2$ admixture of the Rydberg wave function, i.e. $C^J_{n,l=0,N=2}(R)$, given by

$$F_v = \int \left(\sum_{J,n} \Omega_{ns} C^J_{n,l=0,N=2}(R) \right) \chi_v^*(R) \psi_{scat}(R) R^2 dR \quad (12)$$

with $\psi_{scat}(R)$ being the scattering wave function of the initial open channel and $\chi_v(R)$ the vibrational wave function of the final APC, and Ω_{ns} the Rabi frequency for a Rydberg excitation to the ns state. By assuming that the process is dominated by a single ns Rydberg state, i.e. there is no significant admixture of different principle quantum numbers, then we can drop the sum over n. In addition, we assume a constant transition dipole moment and a constant scattering wave function $\psi_{scat}(R)$. Also, to use the standard two-photon scheme for the Rydberg excitation, the final state should have a significant contribution of the s or d-partial waves. This is estimated by the weight of a given partial wave of the Rydberg electron wave function equation (11) integrated over the

vibrational wave function, defined as

$$W_{n,l} = \int \chi_v^*(R) \mathcal{C}_{n,l}(R) \chi_v(R) R^2 dR \quad (13)$$

with $\sum_{n,l} W_{n,l} = 1$. These integrated weights of the s and d-partial waves should be approximately larger than 0.05 in order to be able to create these molecules experimentally. Since KRb is experimentally prepared either in its ground state $N = 0$ or in the $N = 2$ excited state, we have also to analyze the weight of a given rotational partial wave of the KRb wave function equation (10) integrated over the vibrational wave function, defined as

$$W_N = \int \chi_v^*(R) \mathcal{C}_N(R) \chi_v(R) R^2 dR \quad (14)$$

with $\sum_N W_N = 1$. Finally, we also estimate the orientation, alignment and electric dipole moment of the bound vibrational states by

$$\langle \chi_v | X_{ryd} | \chi_v \rangle = \int \chi_v^*(R) X_{ryd}(R) \chi_v(R) R^2 dR \quad (15)$$

with $X = O, A, D$ for the orientation alignment and electric dipole moment, respectively. The expressions of the R-dependent orientation alignment and electric dipole moment, $O_{ryd}(R)$, $A_{ryd}(R)$, $D_{ryd}(R)$, are given in equations (8), (9) and equation (7), respectively.

4. Potential curves, Franck–Condon factors and discussions

In this section, we describe the adiabatic electronic potential energy curves evolving from an ns or nd Rydberg state, which could be used experimentally in the protocol described above to create a TURM.

4.1. K Rydberg excitation

Let us start analyzing the K–KRb Rydberg TURM. The APCs of the TURM formed by K($n = 56$, $l \geqslant 3$) and the KRb in the ground state are presented in figure 2(a). Due to the oscillatory behavior of the Rydberg electron wave function, these APCs oscillate as the distance between the diatomic molecules and Rb$^+$ increases. The two lowest-lying APCs show potential wells with depths up to 1 GHz. The K(58s)–KRb ($N = 2$) APC can be identified among these electronic states as the horizontal line with energy close to -0.1 GHz in figure 2(a). In figure 2(b), we observe that this APC interacts most strongly with other electronic states evolving from K($n = 56$, $l \geqslant 3$)–KRb($N = 0$), near the avoided crossings. For this APC, the outermost well is the deepest one with a depth of approximately ~30 MHz. Most important, each of these potential minima can accommodate at least one vibrational bound state, whose wave functions squared, shifted to the corresponding vibrational energies, are shown in figure 2(b). As an example, we provide the energy spacing of the two lowest-lying vibrational levels, $\omega_{0-1} \sim 6.9$ MHz, see figure 2(b). Within this APC, the polar diatomic molecule is neither oriented nor aligned, due to the small contribution of odd rotational states to the total electronic wave function,
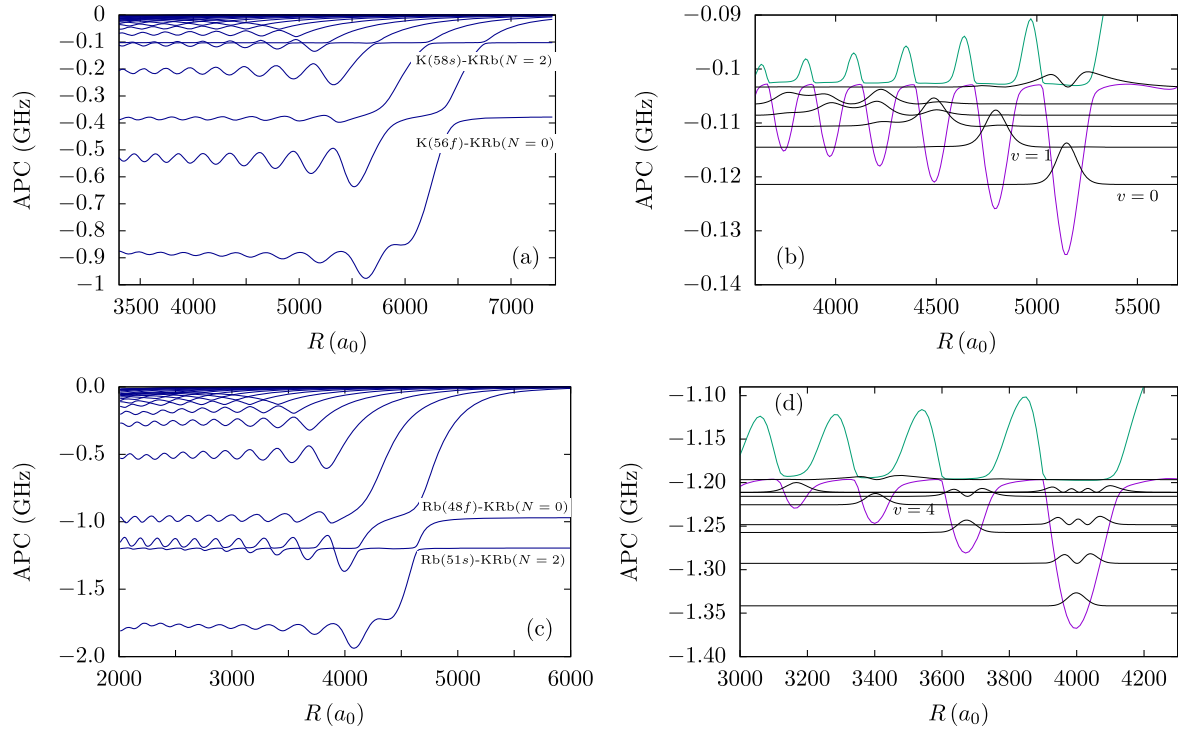
Figure 2. (Top panels) (a) The $M_J = 0$ APC curves for the K–KRb TURM, evolving from K($n = 56, l \geqslant 3$)–KRb(N = 0) limit and K(58s)–KRb(N = 2) limit, (b) details of the APC curves, near the K(58s)–KRb(N = 2) dissociation threshold; (bottom panels) (c) the $M_J = 0$ APC curves for the Rb–KRb TURM, evolving from Rb($n = 54, l \geqslant 3$)–KRb(N = 0) limit and Rb($n = 51s$)–KRb(N = 2) limit, (d) details of the APC curves, near the Rb($n = 51s$)–KRb(N = 2) dissociation threshold. The squared vibrational wave functions, shifted to the corresponding vibrational energies, are shown, for visualization and to illustrate the resolution in the vibrational spacing. Due to appreciable mixing of the K(58s) and Rb(51s) with the respective degenerate manifolds, two-photon excitation to these levels can form the TURM.

Table 1. For the K(58s)–KRb(N = 2) APC: vibrational energies, vibrational spacing, orientation, alignment, and electric dipole moment (in atomic units) of the two lowest lying vibrational states of the K(58s)–KRb(N = 2) APC in figure 2(b).

v	E (GHz)	$\Delta E_{v,v+1}$ (MHz)	$\langle \chi_v \lvert O \rvert \chi_v \rangle$	$\langle \chi_v \lvert A \rvert \chi_v \rangle$	$\langle \chi_v \lvert D \rvert \chi_v \rangle$
0	−0.12140	6.91	0.040	0.351	3656.07
1	−0.11449	3.85	0.039	0.362	3234.38

see table 1. At these vibrational levels, TURM possesses large permanent electric dipole moments. This electric dipole moment is of the same order of magnitude as the one experimentally observed for the ultralong range Rydberg molecules where the perturber is a ground state atom [30, 31] and here comes about from the near resonance of the Rydberg electron and KRb rotational energies.

Figure 3(a) shows the weighted Franck–Condon factors (12) for the six vibrational bound states of the APC K(58s)–KRb(N = 2) in figure 2(b). All the bound vibrational states present similar values for this weighted Franck–Condon factor, and its dependence on the vibrational quantum number illustrates their nodal structure. The integrated weights of the rotational states of KRb for the vibrational state $v = 1$, i.e. the vibrational state located on the second outermost well of the APC, are shown in figure 3(b). Three rotational partial weights $N = 0$, 1, and 2 contribute to the total wave function,

the contribution from the $N = 0$ rotational state being the dominant one. The small contribution of the $N = 1$ rotational state justifies the lack of orientation of KRb with the APC K(58s)–KRb(N = 2). The weights of the partial waves of the Rydberg electron wave function integrated with the vibrational wave functions, see equation (13), for the vibrational state $v = 1$ of the APC are presented in figure 2(c). For this vibrational bound state, many partial waves with $l \geqslant 3$ have an integrated weight larger than 1%, indicating that they have a significant contribution from the K(56, $l > 3$)–KRb(N = 0) APC. The avoided crossing between the K(58s)–KRb(N = 2) APC and the APC evolving from K(56, $l > 3$)–KRb(N = 0) is manifested in the significant contribution of the s-partial wave ($l = 0$), e.g. the integrated weight over the vibrational wave function for this $v = 1$ vibrational bound state is 12%. The large weighted Franck–Condon factors, combined with the large contributions from the Rydberg state K(58s) guarantee that these molecules can be created by the standard two-photon absorption scheme if KRb is in its rotational states $N = 0$ or $N = 2$.

4.2. Rb Rydberg excitation

We explore now the electronic structure of the TURM formed by exciting the rubidium atom, i.e. the Rb–KRb TURM. The APCs evolving from the Rydberg degenerate manifolds Rb($n = 46, l \geqslant 3$) and neighboring quantum-defect states are presented in figure 4. Among these APCs, we identify
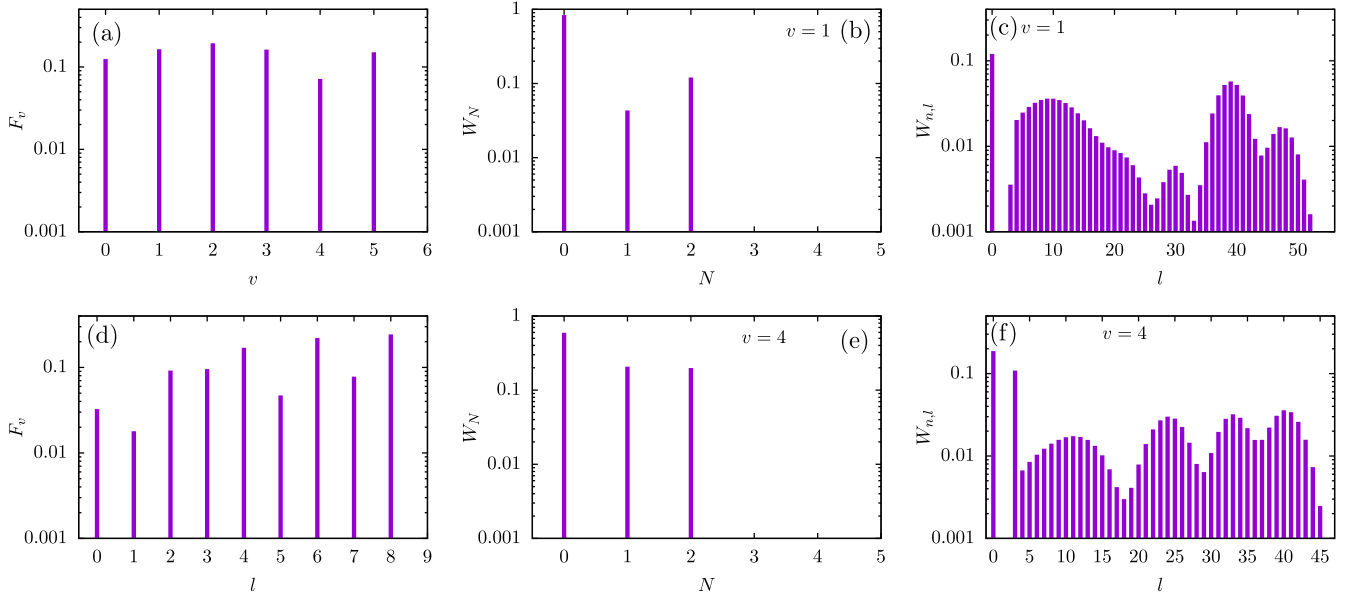
Figure 3. (Top panels) (a) Weighted Franck–Condon factors, equation (12) in the electronic state evolving from K(58s)–KRb($N = 2$); (b) integrated weight of the rotational states equation (10) of K–KRb TURM in the $\nu = 1$ in the most outerwell in figure 2(b); (c) integrated weight of the l-partial waves, equation (11), of K–KRb TURM in the $\nu = 1$ in the most outerwell in figure 2(b); (bottom panels) (d) F$_\nu$ for vibrational states in the APC evolving from Rb(51s)–KRb($N = 2$); (e) W$_N$ for rotational levels of the Rb–KRb TURM in the $\nu = 4$ level in figure 2(d); (f) W$_{nl}$ of Rb–KRb TURM in the $\nu = 4$ in figure 2(d).
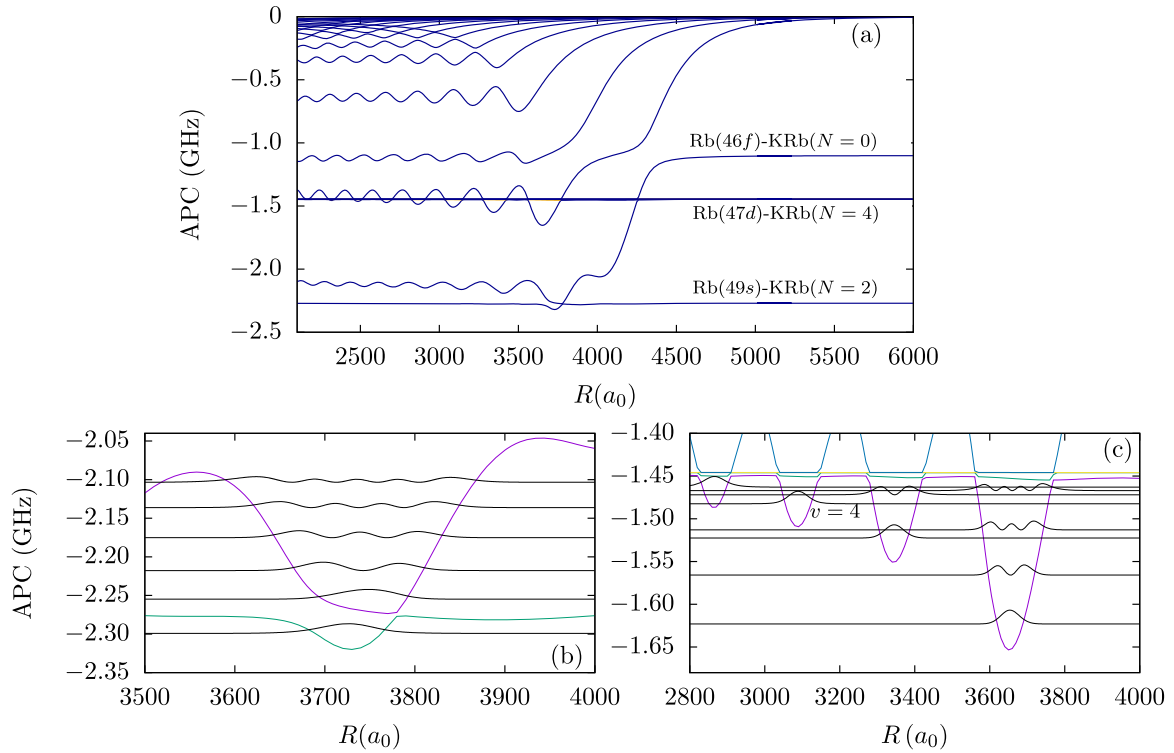

Figure 4. For the Rb–KRb Rydberg TURM, (a) adiabatic electronic potential curves for $M_J = 0$ evolving from the Rydberg state Rb($n = 46$, $l \geqslant 3$) and the KRb in the ground state, Rb(47d)–KRb(N = 4), and Rb(49s)–KRb($N = 2$). (b) Details of the APC evolving from Rb(49s)–KRb($N = 2$) and the neighboring level evolving from Rb($n = 46$, $l \geqslant 3$)–KRb($N = 0$), together with the square of the vibrational wave functions shifted to the corresponding vibrational energies. (c) Details of the APC evolving from Rb(47d)–KRb($N = 4$) and the neighboring level evolving from Rb($n = 46$, $l \geqslant 3$)–KRb($N = 0$). The square of the vibrational wave functions shifted to the corresponding vibrational energies are also shown. Note that the square of the vibrational wave functions is not plotted up to scale: they have been magnified for better visibility.
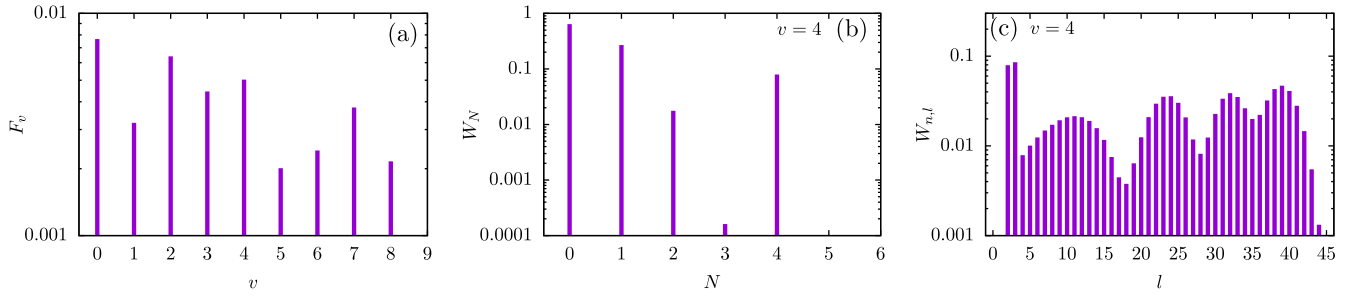
Figure 5. For the Rb–KRb Rydberg TURM, (a) weighted Franck–Condon factors equation (12) for the vibrational bound states of the electronic state evolving from Rb($47d$)–KRb($N = 4$); (b) integrated weight of the rotational states of KRb on the electronic wave function equation (14) of the electronic wave function equation (14) for the vibrational state $v = 4$; (c) integrated weight of the Rydberg l-partial waves in the electronic wave function equation (13) for the vibrational state $v = 4$.

Table 2. For the Rb–KRb Rydberg TURM: vibrational energies, vibrational spacing, orientation, alignment, and electric dipole moment (in atomic units) for selected vibrational bound states of different APCs.

APC	v	E (GHz)	$\Delta E_{v, v+1}$ (MHz)	$\langle \chi_v \vert O \vert \chi_v \rangle$	$\langle \chi_v \vert A \vert \chi_v \rangle$	$\langle \chi_v \vert D \vert \chi_v \rangle$
Rb($47d$)–KRb($N = 4$)	4	−1.4830	10.7	−0.1122	0.4347	2006.2
Rb($49s$)–KRb($N = 2$)	0	−2.2992	21.7	0.2284	0.4173	1857.1
Rb($51s$)–KRb($N = 2$)	4	−1.2255	9.57	−0.0973	0.4348	1877.9

electronic states satisfying the conditions indicated above, which are those evolving from Rb($47d$)–KRb($N = 4$) and Rb($49s$)–KRb($N = 2$), see the horizontal lines, on the scale of the figure, with energies −1.45 GHz and −2.28 GHz, respectively.

The avoided crossing with the Rb($47d$)–KRb($N = 4$) APCs, gives rise to deep potential wells having several vibrational bound states, whose squared wave functions are presented in figure 4(b). The weighted Franck–Condon factors of the nine vibrational bound states of this potential are shown in figure 5(a). For all these states, the weighted Franck–Condon factors are small, and again their dependence on the vibrational quantum number resembles the nodal structure of the vibrational wave function. For the $v = 4$ vibrational state, we present the integrated weights of the rotational wave function in figure 5(b). There are four field-free rotational states of KRb contributing to the wave function, the $N = 0$ contribution being the dominant one due to the avoided crossing. Within this vibrational bound state KRb is anti-oriented. The integrated weights of the partial waves of the Rydberg electron wave function show a dominant contribution for the $l \geqslant 3$ partial waves for the low-lying vibrational states. This indicates that these vibrational bound states are mainly from the APC evolving from the degenerate manifold Rb($n = 46$, $l \geqslant 3$) because they are energetically far from the avoided crossing.

For higher excited vibrational states, i.e. as their energies approach the avoided crossing region, the contribution of the d-wave increases and becomes the largest one. For instance, the integrated weights for the $v = 4$ vibrational level are presented in figure 5(c). The wave function of this fifth vibrational level has around 7.9% contribution of the d-wave, which becomes even larger for higher excitations. This bound state has a vibrational spacing of 10 MHz with respect to the

upper neighboring vibrational states, see table 2, and of 30 MHz with respect to the lower lying one. In addition, it has a large electric dipole moment, but it is weakly anti-oriented and aligned. We can conclude that the TURM molecule could be experimentally created from the quantum-defect state Rb($47d$) if KRb is in the excited rotational state KRb($N = 4$).

The two APCs evolving from Rb($49s$)–KRb($N = 2$) and the neighboring state from the Rb($n = 46$, $l \geqslant 3$)–KRb($N = 0$) manifold, see figure 4(c), can accommodate up to six vibrational bound states with energy spacings ranging from 50 MHz to 35 MHz. The broad avoided crossing between these two APCs gives rise to a non-adiabatic coupling, and, as a consequence, only the lowest-lying vibrational state is stable, whereas the excited ones, i.e. those lying on the upper APC of figure 4(c), will decay and the TURM will dissociate. The weighted Franck–Condon factor to this lowest-lying vibrational state is 0.4, implying a favorable photoassociation rate. For this vibrational state, the integrated weight of the rotational state of KRb is presented in figure 6(a). This vibrational state has a significant contribution of the field-free $N = 0$ and $N = 2$ rotational states, but the KRb shows a moderate alignment, see table 2. Due to the contribution of the $N = 1$ rotational state, the diatomic molecule is weakly oriented, see also table 2. The integrated weights of the partial waves of the Rydberg electron wave function are presented in figure 6(b), where the s-wave has the dominant contribution of 31%. Due to these properties, we can conclude that the TURM molecule could be experimentally created from the quantum-defect state Rb($49s$) if KRb is in the $N = 2$ rotational state.

For completeness, we present in figure 2(c) the electronic structure of the TURM formed from the Rydberg degenerate
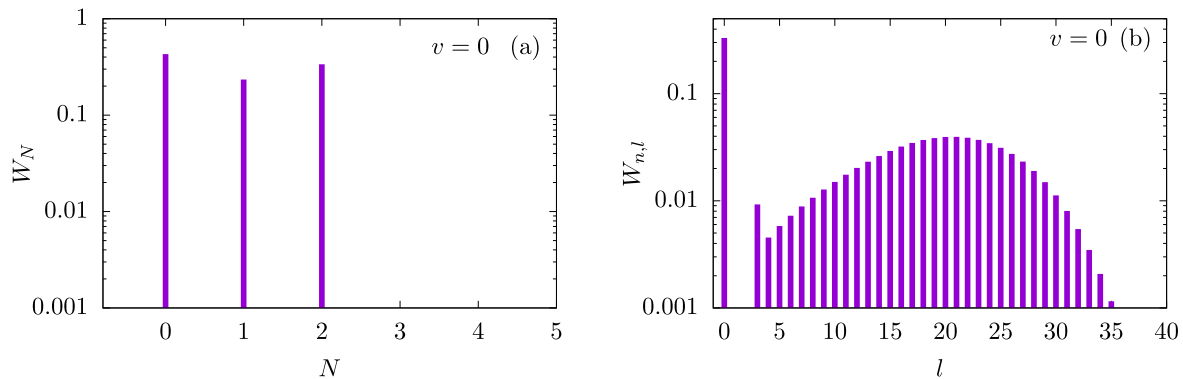
Figure 6. For the $v = 0$ vibrationl state in the electronic state evolving from Rb(49s)–KRb($N = 2$) Rydberg TURM, (a) integrated weight of the rotational states of KRb and (b) integrated weight of the l-partial waves in the electronic wave function of this vibrational state $\nu = 0$.

manifolds Rb($n = 54$, $l \geqslant 3$) and the ground-state diatomic molecule. In this configuration, we encounter the adiabatic electronic state evolving from the Rb(51s)–KRb($N = 2$), which suffers an avoided crossing with an APC evolving from Rb($n = 54$, $l \geqslant 3$)–KRb($N = 0$), see figure 2(d). The potential wells accommodate 8 vibrational bound states, whose wave functions are shown figure 2(d). As in the previous cases, we present in figure 3(d) the weighted Franck–Condon factor of these vibrational states. The low-lying vibrational bound levels are far from the avoided crossing, and they do not show a significant contribution of the s-wave Rydberg wave function. As the energy of these vibrational states increases, the avoided crossing strongly affects their properties. In particular, for the fourth vibrational state, the integrated weight of the Rydberg partial wave to the electronic wave function are presented in figure 3(f). The Rydberg s-wave has the dominant contribution with 19%, which is even larger for higher excited vibrational states. In addition, the integrated weights of the KRb rotational states to the $v = 4$ vibrational bound state are shown in figure 3(e). Within this vibrational state the KRb is antioriented. The properties of this vibrational bound state are shown in table 2.

5. Conclusions

We have investigated triatomic ultralong-range Rydberg molecules formed by a Rydberg rubidium or potassium atom and a KRb diatomic rotational molecule. We have explored a regime where the dipole interaction of the Rydberg electron with the diatomic polar molecule induces a coupling between the quantum defect Rydberg states and the nearest degenerate hydrogenic manifold. Due to this induced coupling, the adiabatic potential wells evolving from the hydrogenic like Rydberg manifold acquire s- and d-wave admixture from the corresponding Rydberg quantum defect states. As a consequence, an experimental protocol with the conventional two-photon excitation can be employed to create TURM [13, 30, 31] could be used to prepare the Rydberg triatomic Rydberg molecules described here. To get a measurable photo-association rate, the densities of the atomic and molecular gases must be large enough such that there is a reasonable probability of finding on average one molecule inside the Rydberg orbit. For Rb–KRb

TURM photo-association, a relatively dilute gas of Rb with density $\sim 1 \times 10^{12}\,\mathrm{cm}^{-3}$ overlapping with a gas of KRb molecules in their electronic and vibrational ground state prepared in the $N = 2$ rotational state with a density of $2 \times 10^{12}\,\mathrm{cm}^{-3}$ [32] has on average ~ 0.1 KRb molecules within a Rb Rydberg orbit. Since it is based on the dipole-induced coupling between different Rydberg states, this experimental protocol is ubiquitous and could be applied to any pair of species forming these ultralong-range Rydberg molecules. Optical tweezers may provide another platform to create the TURM. Overlap of single molecule trap [33] and atom tweezer [34, 35], which can be excited into Rydberg states, offer the opportunity to form triatomic Rydberg molecules at the right separation.

ORCID iDs

Rosario González-Férez ⓘ https://orcid.org/0000-0002-8871-116X
Peter Schmelcher ⓘ https://orcid.org/0000-0002-2637-0937
H R Sadeghpour ⓘ https://orcid.org/0000-0001-5707-8675

References

[1] Allard N and Kielkopf J 1982 *Rev. Mod. Phys.* **54** 1103–82
[2] Szudy J and Baylis W 1996 *Phys. Rep.* **266** 127–227
[3] Amaldi E and Segre E 1934 *Il Nuovo Cimento* **11** 145–56
[4] Fermi E 1934 *Il Nuovo Cimento* **11** 157–66

[5] Lukin M D, Fleischhauer M, Cote R, Duan L M, Jaksch D, Cirac J I and Zoller P 2001 *Phys. Rev. Lett.* **87** 037901

[6] Schmidt R, Sadeghpour H R and Demler E 2016 *Phys. Rev. Lett.* **116** 105302

[7] Camargo F *et al* 2018 *Phys. Rev. Lett.* **120** 083401

[8] Saffman M, Walker T G and Mølmer K 2010 *Rev. Mod. Phys.* **82** 2313–63

[9] Carr L, DeMille D, Krems R and Ye J 2015 Focus Issue: Focus on new frontiers of cold molecules research and references there *New J. Phys.* **17**

[10] Greene C H, Dickinson A S and Sadeghpour H R 2000 *Phys. Rev. Lett.* **85** 2458

[11] Hamilton E L, Greene C H and Sadeghpour H R 2002 *J. Phys. B: At. Mol. Opt. Phys.* **35** L199

[12] Chibisov M I, Khuskivadze A A and Fabrikant I I 2002 *J. Phys. B: At. Mol. Opt. Phys.* **35** L193

[13] Bendkowsky V, Butscher B, Nipper J, Shaffer J P, Löw R and Pfau T 2009 *Nature* **458** 1005

[14] Fermi E and Teller E 1947 *Phys. Rev.* **72** 399

[15] Crawford O H 1967 *Proc. Phys. Soc.* **91** 279–84

[16] Clark C W 1979 *Phys. Rev.* A **20** 1875–89

[17] Sadeghpour H R, Bohn J L, Cavagnero M J, Esry B D, Fabrikant I I, Macek J H and Rau A R P 2000 *J. Phys. B: At. Mol. Opt. Phys.* **33** R93–140

[18] Rittenhouse S T and Sadeghpour H R 2010 *Phys. Rev. Lett.* **104** 243002

[19] Rittenhouse S T, Mayle M, Schmelcher P and Sadeghpour H R 2011 *J. Phys. B: At. Mol. Opt. Phys.* **44** 184005

[20] González-Férez R, Sadeghpour H R and Schmelcher P 2015 *New J. Phys.* **17** 013021

[21] Mayle M, Rittenhouse S T, Schmelcher P and Sadeghpour H R 2012 *Phys. Rev.* A **85** 052511

[22] Aguilera-Fernández J, Sadeghpour H R, Schmelcher P and González-Férez R 2015 *J. Phys.: Conf. Ser.* **635** 012023

[23] Kuznetsova E, Rittenhouse S T, Sadeghpour H R and Yelin S F 2011 *Phys. Chem. Chem. Phys.* **13** 17115–21

[24] Kuznetsova E, Rittenhouse S T, Sadeghpour H R and Yelin S F 2016 *Phys. Rev.* A **94** 032325

[25] Kuznetsova E, Rittenhouse S T, Beterov I I, Scully M O, Yelin S F and Sadeghpour H R 2018 *Phys. Rev.* A **98** 043609

[26] Ni K K, Rosenband T and Grimes D D 2018 *Chem. Sci.* **9** 6830–8

[27] Ni K K, Ospelkaus S, De Miranda M H G, Peér A, Neyenhuis B, Zirbel J J, Kotochigova S, Julienne P S, Jin D S and Ye J 2008 *Science* **322** 231–5

[28] Ni K K, Ospelkaus S, Nesbitt D J, Ye J and Jin D S 2009 *Phys. Chem. Chem. Phys.* **11** 9626–39

[29] Marinescu M, Sadeghpour H R and Dalgarno A 1994 *Phys. Rev.* A **49** 982

[30] Li W *et al* 2011 *Science* **334** 1110–4

[31] Booth D, Rittenhouse S T, Yang J, Sadeghpour H R and Shaffer J P 2015 *Science* **348** 99–102

[32] De Marco L, Valtolina G, Matsuda K, Tobias W G, Covey J P and Ye J 2019 *Science* **363** 853–6

[33] Anderegg L, Cheuk L W, Bao Y, Burchesky S, Ketterle W, Ni K K and Doyle J M 2019 *Science* **365** 1156–8

[34] Bernien H *et al* 2017 *Nature* **551** 579–84

[35] Wilson J, Saskin S, Meng Y, Ma S, Burgers A and Thompson J 2019 (arXiv:1912.08754)